*The FASEB Journal*

FASEB
Federation of American Societies for Experimental Biology

RESEARCH ARTICLE OPEN ACCESS

# Ocular Risks of Spaceflight and a Path to Prevention: Targeting Mitochondria–ER Stress With Low-Intensity Ultrasound

Jee Hoon Lee[1] | Hankyung Kim[1,2,3] | Dae Yu Kim[1,2,3]

[1]Inha Research Institute for Aerospace Medicine, Inha University, Incheon, Republic of Korea | [2]Department of Electrical and Computer Engineering, College of Engineering, Inha University, Incheon, Republic of Korea | [3]Center for Sensor Systems, Inha University, Incheon, Republic of Korea

**Correspondence:** Dae Yu Kim (dyukim@inha.ac.kr)

**Received:** 11 August 2025 | **Revised:** 17 December 2025 | **Accepted:** 6 January 2026

**Keywords:** corneal degeneration | endoplasmic reticulum (ER) stress | inter-organelle communication | low-intensity ultrasound (LIUS) | microgravity | mitochondria-associated membranes (MAMs) | mitochondrial dysfunction | spaceflight

## ABSTRACT

The cornea is highly susceptible to spaceflight-induced stress, compromising visual acuity and mission safety. Here, we identify endoplasmic reticulum (ER) and mitochondrial dysfunction as key mediators of corneal degeneration under simulated microgravity (SMG). SMG exposure led to corneal epithelial thinning, reduced nerve fiber density, and delayed wound healing. Multi-omics profiling and cellular assays revealed aberrant ER–mitochondrial crosstalk, characterized by excessive formation of mitochondria-associated membranes (MAMs) and activation of stress signaling pathways. Notably, treatment with low-intensity ultrasound (LIUS) restored corneal epithelial integrity by modulating MAM dynamics, alleviating organelle stress, and normalizing cellular homeostasis. These findings identify a novel molecular axis in microgravity-induced ocular degeneration and propose LIUS as a deployable, non-invasive countermeasure for preserving corneal health during deep spaceflight.

## 1 | Introduction

The advent of the space age has enabled human exploration of outer space, accompanied by increasingly prolonged space missions. However, space represents an extreme and unfamiliar environment characterized by factors such as cosmic radiation and microgravity, both of which profoundly affect human physiology. These include muscle and bone loss, immune system dysregulation, and cardiovascular alterations [1–3]. Importantly, spaceflight has also been associated with the development of a range of ocular abnormalities, including spaceflight-associated neuro-ocular syndrome (SANS) and others [4, 5]. Among ocular tissues, the cornea—the transparent, outermost layer of the eye—is particularly vulnerable to spaceflight-induced environmental afflictions. Additionally, in the microgravity environment of space, the redistribution and prolonged suspension of airborne particulates increase the likelihood of corneal exposure, thereby elevating risks of abrasion, inflammation, and infection. These complications may cause visual disturbances that hinder astronaut performance and mission safety. Indeed, over 30% of astronauts aboard the International Space Station (ISS) have reported symptoms of dry eye disease, such as ocular redness, itchiness, stinging, and fatigue [5, 6]. Although previous studies suggest that oxidative stress and mitochondrial dysfunction under microgravity may underlie these symptoms [7, 8], the precise pathophysiological mechanisms remain poorly defined. Given the limited availability of medical interventions in space, there is an urgent need to identify the molecular underpinnings of spaceflight-induced corneal injury and develop targeted countermeasures.

Recent multi-omics analyses from NASA's GeneLab platform (http://genelab.nasa.gov/) have revealed that mitochondrial dysfunction is a common hallmark across multiple tissues, including

ocular tissues, under spaceflight conditions [9, 10]. Mitochondria are critical for ATP production and maintaining cellular homeostasis, and mitochondrial dysfunction—characterized by the loss of membrane potential, release of cytochrome c, and overproduction of reactive oxygen species (ROS)—can trigger cell death [11, 12]. Mitochondria maintain close physical and functional interactions with the endoplasmic reticulum (ER) through contact sites known as mitochondria-associated membranes (MAMs). These specialized structures regulate calcium signaling, lipid metabolism, and cellular stress responses and are increasingly recognized as central hubs in inter-organelle communication [13–15]. Under conditions of chronic ER stress, excessive MAM formation can lead to pathological calcium overload in mitochondria, resulting in oxidative injury and membrane depolarization [16–18]. Dysfunctional MAMs have been implicated in various ocular diseases, including corneal dystrophy, retinal detachment, and glaucoma [13, 19, 20]. Although ongoing research continues to explore the role of mitochondrial dysfunction in spaceflight-associated ocular abnormalities, the mechanistic link between mitochondrial damage and corneal degeneration under microgravity remains largely undefined. Elucidating this link and developing interventions to suppress mitochondrial dysfunction are essential for preventing vision-related complications during space missions.

Ultrasound, mechanical sound waves with frequencies above 20 kHz, have emerged as a versatile tool in biomedical science due to its non-invasive nature and highly tunable physical parameters, including frequency, duty cycle, acoustic intensity, and energy. Its applications span a broad spectrum, encompassing diagnostic imaging, targeted drug delivery, and therapeutic stimulation [21, 22]. Notably, low-intensity ultrasound (LIUS, 20–1000 mW/cm$^2$) has shown promise as a therapy for a variety of pathological conditions, including uses in pain relief, thrombosis treatment, fracture healing, osteoporosis, osteoarthritis, and tissue regeneration [23–27]. In ophthalmology, LIUS has been reported to protect retinal ganglion cells (RGCs) by enhancing yes-associated protein (YAP) expression, modulating ocular movements during sleep, and facilitating the trans-corneal delivery of macromolecules [28–30]. Although the cellular mechanisms of LIUS are still being clarified, accumulating evidence indicates that it can regulate cell proliferation, calcium signaling, inflammatory responses, and ROS generation [31, 32]. In cardiovascular models, for example, LIUS at 2.5 W/cm$^2$ has been shown to prevent apoptotic signaling via modulation of the JNK pathway, while at 47.12 mW/cm$^2$, LIUS suppressed endothelial-to-mesenchymal transition by reducing ROS accumulation [33, 34]. However, not all effects of LIUS are beneficial. Under certain conditions, LIUS exposure may exacerbate ER stress and mitochondrial dysfunction, potentially leading to cell death [35, 36]. These contradictory findings underscore the importance of identifying the optimal LIUS parameters—such as the optimal energy dose, frequency, and treatment duration—that maximize therapeutic outcomes while minimizing adverse effects.

In the present study, we investigated the effects of simulated microgravity (SMG) on ocular cells and evaluated the therapeutic potential of LIUS. We found that SMG exacerbates damage in corneal epithelial and neural cells by intensifying ER stress and mitochondrial dysfunction, accompanied by the excessive formation of MAMs. Remarkably, LIUS treatment suppressed the aberrant formation of MAMs, alleviating ER stress and mitochondrial damage and promoting cell survival. These findings reveal a novel molecular mechanism underlying microgravity-induced corneal injury and identify LIUS as a promising, non-invasive therapeutic strategy to preserve ocular health during space missions.

## 2 | Materials and Methods

### 2.1 | Organotypic Cultures

Organotypic eye cultures were prepared from adult C57BL/6 mice following previously reported protocols [37, 38], with minor modifications. In brief, the mice were anesthetized, and their eyes were enucleated. Subsequently, the eyes were placed in Hanks' balanced salt solution (HBSS) containing hydroxyethyl piperazine ethane sulfonic acid (HEPES, 10 mM), and the remaining meninges were carefully removed. To simulate microgravity, the enucleated eyeballs were placed in 0.5 mL microtubes filled completely with Neurobasal medium containing B27 (2%), sodium pyruvate (1%), penicillin/streptomycin (1%), and GlutaMAX (1%)—and then incubated under 1G or $10^{-3}$G conditions for up to 7 days. During SMG, the culture medium was changed every 2–3 days.

### 2.2 | Cell Culturing

Human corneal epithelial cells (HCE cells) were purchased from ATCC (Manassas, VA, USA). The cells were plated onto Dulbecco's modified Eagle's medium (DMEM) containing FBS (10%) and penicillin/streptomycin (1%) in tissue-culture plates, which were then incubated at 37°C with 5% $CO_2$.

### 2.3 | Microgravity Simulation

To simulate microgravity, cells and eyeballs were cultured under normal gravity (1 ×g; 1G) or simulated microgravity ($10^{-3}$×g; SMG) using a Gravite device (Space Bio-Laboratories, Japan). This device produces an environment replicating spaceflight conditions ($10^{-3}$×g) by rotating a sample around two axes [39, 40]. The device provides four rotation programs—Mode A: ×4 rpm; Mode B: ×3 rpm; Mode C: ×2 rpm; and Mode D: ×1 rpm—of which Mode C (×2 rpm) is recommended for adherent cell culture [39, 41–43]. To prevent fluid shear stress, culture flasks or tubes were completely filled with the appropriate medium, ensuring the absence of air bubbles before mounting on the Gravite device. Microgravity exposure was conducted in Mode C within a humidified $CO_2$ incubator maintained at 37°C and 5% $CO_2$. Culture media were replaced every 2–3 days for up to 7 days in organotypic cultures and up to 14 days in cell cultures.

### 2.4 | Experimental Setup for LIUS Treatment

Low-intensity ultrasound was applied from the bottom of the culture dish using a piezoelectric transducer operating at either 28 or 40 kHz. A 35 mm culture dish containing either control or SMG-exposed HCE cells was placed directly on the transducer, with approximately 1 mL of an ethanol-based sanitizer gel applied between the dish and the transducer to ensure acoustic coupling. The acoustic impedance of the sanitizer gel was nearly equivalent to that of the culture dish, minimizing

reflection and allowing approximately 94.15% of the ultrasound energy to be transmitted to the cells. To maintain consistent positioning of the dish and gel, a custom-designed dish holder was fabricated using 3D-printed silicone rubber. The entire culture dish–transducer assembly was placed inside a standard $CO_2$ incubator during LIUS exposure. The LIUS treatment was conducted for 30 min at frequencies ranging from 10 to 40 kHz, with voltage amplitudes varied between 1 and 30 Vpp. The input waveform was generated using a function generator (UTG-2025A, Uni-Trend, China) and amplified via a linear amplifier (WMA-300, Falco Systems, the Netherlands). Cell temperature was continuously monitored during ultrasound exposure using epoxy-encapsulated NTC thermistors (NTCLE413, Vishay, PA). Temperature values were calculated based on real-time resistance measurements using the Steinhart–Hart equation.

### 2.5 | Data Collection

The RNAseq eye tissue transcriptome datasets from Rodent Research-1 (RR-1) and Rodent Research-3 (RR-3) missions were obtained from NASA's GeneLab data repository (https://genelab.nasa.gov/). The datasets are accessible under the following GeneLab Data System (GLDS) identifiers: GLFD-100 from RR-1 and GLDS-162 from RR-3. Detailed descriptions of each mission, including associated biological conditions and experimental protocols, are available within the respective dataset's metadata on GeneLab (Table S1). Differential gene expression analyses comparing *Flight* and *Ground Control* samples were conducted separately for each dataset using publicly available transcriptome data from each dataset identifier. Genes with an adjusted $p$-value $<0.05$ and absolute $\log_2$ fold change $>1$ ($|\log_2 FC|>1$) were considered significantly differentially expressed.

### 2.6 | Enrichment Analysis of Genes and Pathways of Differentially Expressed Genes

A pathway enrichment analysis was performed on the differentially expressed genes (DEGs) using gene set enrichment analysis (GSEA) via the g:Profiler platform (https://biit.cs.ut.ee/gprofiler/gost). Genes were input as an ordered query based on their differential expression values, and gene ontology (GO) terms—including Molecular Function (MF) and Cellular Component (CC) terms—were selected as enrichment categories. The enrichment results were exported as a GEM file and imported into Cytoscape (https://cytoscape.org) for visualization and interpretation using the EnrichmentMap plugin. To reduce network complexity and enhance interpretability, filtering thresholds were applied: nodes were filtered using a FDR cutoff of $p<0.05$, and edges were filtered using a Jaccard similarity coefficient cutoff of $<0.05$.

### 2.7 | Real-Time Reverse Transcription–Quantitative Polymerase Chain Reaction Analysis

Total RNA was extracted using RNAiso Plus (TaKaRa, Japan) following the manufacturer's protocol. Complementary DNA (cDNA) synthesis was subsequently performed with Moloney murine leukemia virus reverse transcriptase and oligo(dT) primers (CellSafe, Korea). Quantitative polymerase chain reaction (qPCR) was carried out on a CFX real-time PCR system (Bio-Rad, Hercules, CA) using SYBR qPCR master mix (TaKaRa, Japan), according to the manufacturer's guidelines. The primer sequences utilized for qPCR (Bioneer, Korea) are listed in Table S2.

### 2.8 | Western Blotting

Cells were lysed in RIPA buffer (0.15 M NaCl, 1% Triton X-100, 50 mM Tris–HCl at pH 7.5, 1% sodium deoxycholate, 0.1% SDS, and 2 mM EDTA at pH 8.0), supplemented with a protease inhibitor cocktail (ATTO, Japan), and incubated at 4°C for 30 min. The extracted proteins were separated by SDS-PAGE and transferred onto nitrocellulose membranes. After blocking, the membranes were probed with primary antibodies followed by horseradish peroxidase–conjugated secondary antibodies. Immunoreactive bands were visualized using an enhanced chemiluminescence detection system (Bio-Rad). Primary antibodies included rabbit anti-zonular occludens-1 (ZO-1) and mouse anti-matrix metalloproteinase-9 (MMP-9) (Thermo Fisher Scientific, Waltham, MA), as well as mouse anti-vascular endothelial growth factor (VEGF) and mouse anti-beta-actin (Santa Cruz Biotechnology, Santa Cruz, CA).

### 2.9 | Immunofluorescence

Eye sections were permeabilized with 0.2% Triton X-100 for 30 min and subsequently blocked in 1% bovine serum albumin (BSA) for 1 h before being incubated overnight at 4°C with anti-TUBB3 (Cell signaling, MA) and anti-ZO-1 (Thermo Fisher Scientific) antibodies diluted in 1% BSA and 0.2% Triton X-100 in phosphate-buffered saline (PBS). The sections were then washed in PBS before being incubated with secondary antibodies (Invitrogen, Carlsbad, CA) for 1 h. The sections were again washed in PBS and then mounted with Vectashield medium containing 4′,6-diamidino-2-phenylindole (DAPI; Vector Laboratories, Burlingame, CA).

### 2.10 | Subcellular Fractionation

Endoplasmic reticula, mitochondria, and MAMs were isolated from SMG- or 1G-exposed HCE cells following previously described protocols [44] with minor modifications. Briefly, cells at ~90% confluence were harvested from 20 dishes (10 cm) and homogenized using a Dounce tissue grinder (Wheaton, Millville, NJ) in a 75 mM sucrose, 30 mM Tris–HCl at pH 7.4, 225 mM mannitol, 0.1 mM EGTA, isolation buffer. The homogenate was centrifuged twice at 600 $g$ for 10 min to remove nuclei and debris. The resulting supernatant was subjected to centrifugation at 8000 $g$ for 15 min to obtain the crude mitochondrial pellet. After isolating the mitochondrial tissue, the supernatant was then centrifuged at 20 000 $g$ for 1 h, and subsequently at 100 000 $g$ for 1 h. The resulting pellet was resuspended in isolation buffer and designated as the ER fraction, while the supernatant was kept as the cytosolic fraction. To obtain purified MAM fractions and mitochondria, the crude mitochondrial pellet was resuspended in 2 mL of mitochondrial resuspension buffer (5 mM

HEPES at pH 7.4, MRB; 250 mM mannitol, and 0.5 mM EGTA), layered onto 30% Percoll solution, and centrifuged at 100 000 *g* for 30 min. The lower fraction (pure mitochondria) and the intermediate fraction (MAM, located between the light membrane layer and the mitochondrial layer) were carefully collected. The purified mitochondrial fraction was diluted in MRB and subjected to centrifugation at 10 000 *g* for 20 min. The resulting pellet was then resuspended in 300 μL of MRB. The MAM fraction was diluted 10-fold with MRB and subjected to ultracentrifugation at 100 000 *g* for 1 h. The final MAM pellet was then resuspended in a minimal volume of MRB for further analysis.

### 2.11 | Analysis of Mitochondrial Morphology

To visualize mitochondria, cells were incubated with MitoTracker Red CMXRos (Invitrogen) at 37°C for 20 min. Fluorescence imaging was performed using confocal microscopy, and mitochondrial morphology was quantified using the open-source image analysis software CellProfiler (https://cellprofiler.org). Mitochondria were segmented using a global, three-class Otsu thresholding algorithm. Following segmentation, individual mitochondrial objects' morphological parameters, including form factor (a measure of mitochondrial branching), aspect ratio (the proportional relationship between width and height), and solidity (reflecting structural compactness), were quantified and analyzed using three independent biological replicates, with at least 10 cells analyzed per condition in each experiment with a confocal microscope (Zeiss) equipped with a 40× objective (1.10 NA) on a heated stage.

### 2.12 | Flow Cytometry

Simulated microgravity- or 1G-exposed HCE cells were stained with a superoxide indicator, MitoSOX Green (5 μM; Invitrogen), for 30 min at 37°C. The cells were then treated with trypsin and analyzed using the CytoFLEX flow cytometer (Beckman Coulter, Brea, CA).

### 2.13 | Statistical Analysis

The data were plotted using GraphPad Prism 9.5.1. Statistical significance was determined through an unpaired two-tailed Student's *t*-test for pairwise comparisons, and one-way or two-way analysis of variance (ANOVA) for multiple comparisons. Post hoc multiple comparison corrections were performed using the Dunnett method (one-way ANOVA), the Sidak method (two-way ANOVA). A *p*-value of 0.05 was considered statistically significant. The values are presented as mean ± SD.

## 3 | Results

### 3.1 | Simulated Microgravity Promotes Corneal Damage and Impairs Epithelial Wound Healing

To evaluate the impact of SMG on corneal integrity, enucleated mouse eyeballs and HCE cells were incubated under either normal gravity (1G) or SMG conditions for 7 and 14 days, respectively (Figure 1A). Hematoxylin and eosin (H&E) staining revealed that corneal tissues in the SMG-exposed mouse eyeballs exhibited a more fragile structure compared to those in the 1G group. Quantitative analysis further demonstrated that corneal thickness was significantly reduced by approximately 52% under SMG conditions relative to normal gravity (Figure 1B and Figure S1A). Given the importance of corneal epithelium–nerve interactions in maintaining epithelial homeostasis [45, 46], we next assessed corneal innervation using TUBB3 immunofluorescence. In the 1G group, TUBB3-positive nerve fibers displayed intact morphologies and extended throughout the epithelial layers. In contrast, epithelia in the SMG group showed a marked decrease in nerve fiber density (Figure 1C–E). We further investigated epithelial barrier function by analyzing the expression of the tight junction protein ZO-1, which is critical for epithelial structural integrity. Immunofluorescence analysis revealed that ZO-1 expression was reduced in the SMG group relative to the 1G control (Figure 1D,F). In SMG-exposed HCE cells, protein levels of MMP9 and VEGF—molecules known to mediate epithelial barrier breakdown [47, 48]—were found to be consistently upregulated (Figure 1G and Figure S1B). Additionally, cell viability assays revealed a significant reduction in the HCE cell survival under SMG conditions compared to 1G (Figure 1H and Figure S1C), further supporting the notion that SMG exposure compromises corneal epithelial cell health and contributes to tissue damage.

As previous reports have demonstrated that corneal epithelium–neuron crosstalk is essential for proper wound healing [49], we next examined whether SMG impairs epithelial wound healing. A scratch wound assay, performed on confluent HCE monolayers, revealed that while most of the wound area was closed within 48 h in the 1G group, wound closure was significantly delayed in the SMG group (Figure 1I). These findings suggest that SMG not only accelerates corneal damage but also interferes with the normal wound healing process of the corneal epithelium.

### 3.2 | Transcriptomic Analysis of Mouse Eye Tissue Reveals Spaceflight-Induced Mitochondrial and ER Stress Signatures

To investigate whether spaceflight-associated molecular changes occur in ocular tissues, we performed a transcriptomic analysis using publicly available datasets from NASA's GeneLab space omics repository. Previous multi-omics analyses of GeneLab data have reported significant alterations in mitochondrial function, chronic inflammation, and cell cycle regulation across various organs [9]. To extend these findings to ocular tissues, we analyzed two transcriptomic datasets derived from mouse eye tissues collected after spaceflight aboard the ISS. A differential gene expression analysis was performed to identify changes in expression between the spaceflight- and ground control-group mice. Subsequent GO enrichment and GSEA analyses revealed consistent dysregulation of several biological pathways across both datasets (Figure 2A and Table S3). GO enrichment analysis performed using g:Profiler identified 52 and 10 enriched pathways within the molecular function and cellular component categories, respectively (Figure 2B,C). These pathways were further

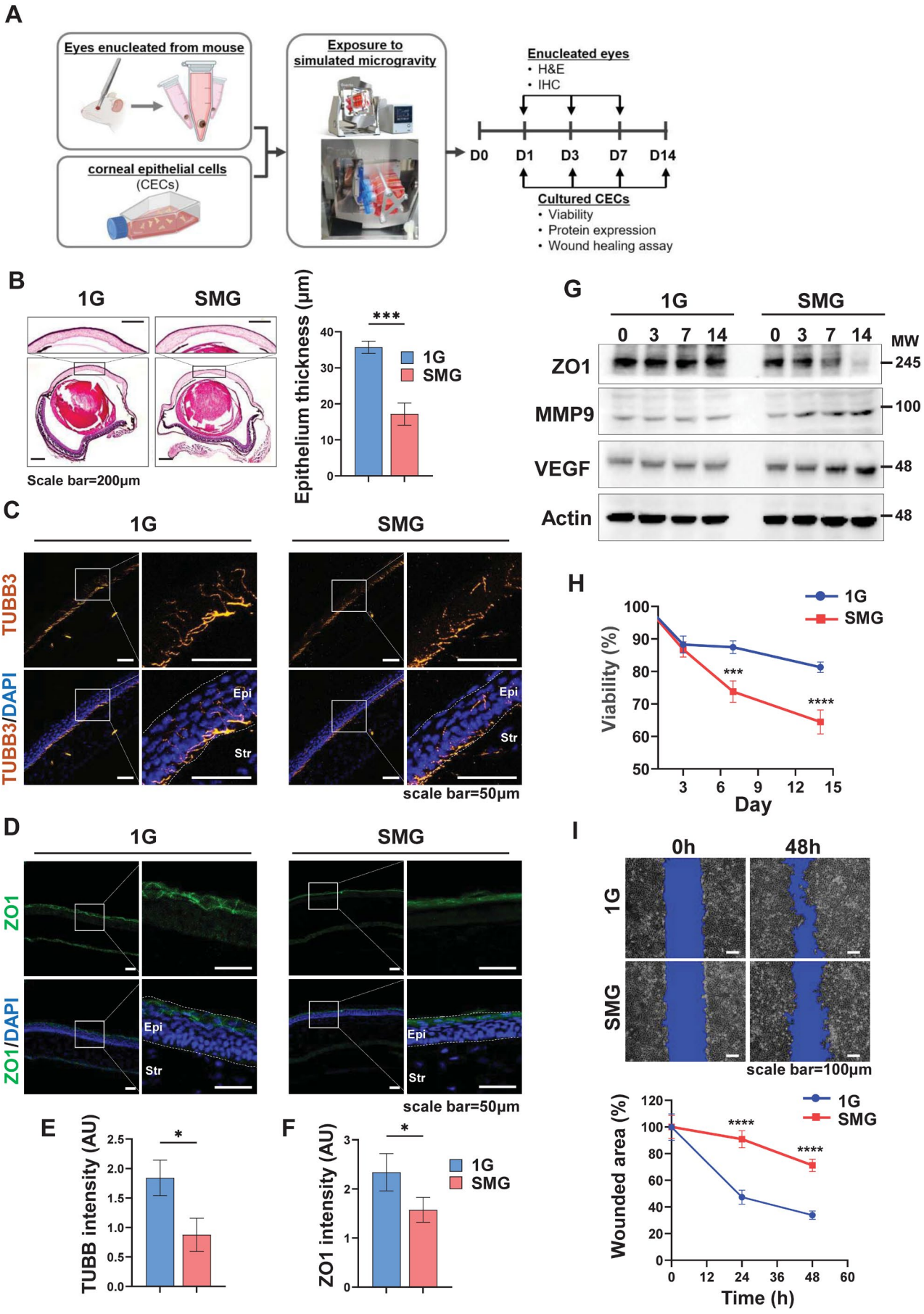


**FIGURE 1** | Legend on next page.

**FIGURE 1** | SMG induces corneal damage and impairs epithelial wound healing. (A) A schematic detailing the experimental design. Enucleated mouse eyeballs and HCE cells were cultured for 7 or 14 days, respectively, under 1G or SMG conditions. (B) Representative H&E-stained corneal sections from 1G- and SMG-exposed eyeballs. Epithelial thickness measurements are shown on the right. Eyes from three mice per group were examined, and data are presented as mean ± SD of three independent experiments. ***$p < 0.001$. (C–F) The confocal immunohistochemistry of corneal sections after 7 days of 1G or SMG treatment, including representative images of TUBB3 (C) and ZO-1 (D) staining. Measurements of fluorescence intensity are shown in (E and F) (Epi, epithelium; Str, stroma). Eyes from three mice per group were examined, and data are representative of three fields of view per group of three independent experiments. *$p < 0.05$. (G) Western blot analysis of selected proteins in HCE cells cultured under 1G or SMG for 14 days. (H) HCE cell viability, measured via the WST-8 assay, after exposure to 1G or SMG for 14 days. Data are presented as mean ± SD of three independent experiments. ***$p < 0.001$; ****$p < 0.0001$. (I) A scratch assay was performed on confluent HCE monolayers followed by a 48-h incubation under 1G or SMG conditions. Representative images (top) and measurements of wound area (bottom) are shown. Data are presented as mean ± SD of three independent experiments. ****$p < 0.0001$.

visualized through Cytoscape network analysis (Figure S2). Notably, genes associated with mitochondrial and ER functions were consistently enriched in spaceflight-exposed samples, aligning with previously reported signatures observed in non-ocular tissues. Given the critical role of ER–mitochondria interactions in maintaining mitochondrial homeostasis, these findings implicate ER stress as a potential contributor to spaceflight-induced mitochondrial dysfunction in ocular tissues.

### 3.3 | SMG Induces ER Stress and Mitochondrial Dysfunction in HCE

Both ER and mitochondrial stress are known contributors to ocular diseases, either independently or through organelle crosstalk [50]. Our transcriptomic analysis of NASA's GeneLab datasets revealed elevated markers of ER stress and mitochondrial dysfunction in eye tissues exposed to spaceflight. Based on these findings, we sought to validate whether similar changes occur in HCE cells under SMG conditions. To this end, HCE cells were cultured under SMG or 1G conditions for 7 days, and the expression of ER stress–related genes and proteins was assessed using qRT-PCR and western blot analysis, respectively. Results showed that both ER stress–associated mRNA and protein levels were significantly greater in SMG-exposed cells than in those maintained under 1G (Figure 3A,B and Figure S3A). We next evaluated whether SMG induces mitochondrial dysfunction in HCE cells. Cells were stained with MitoTracker and imaged to assess mitochondrial morphology. The SMG-treated cells displayed increased mitochondrial fragmentation and instances of abnormal morphology relative to the 1G controls (Figure 3C). This was evident from reductions in aspect ratio and form factor under SMG conditions (Figure 3D). In addition, mitochondrial membrane potential, as measured by tetramethyl rhodamine ethyl ester (TMRE) fluorescence, was significantly reduced (Figure 3E), and mitochondrial ROS levels, as indicated by MitoSOX staining, were markedly increased (Figure 3F). To further confirm SMG-induced mitochondrial dysfunction, we analyzed the expression of two mitochondrial proteins—NADH:ubiquinone oxidoreductase core subunit S3 (NDUFS3) and ATP synthase F1 subunit alpha (ATP5A)—by immunoblotting. Both protein levels were markedly decreased under SMG conditions, supporting that SMG induces mitochondrial impairment (Figure 3G and Figure S3B). Together, these findings demonstrate that simulated microgravity promotes both ER stress and mitochondrial dysfunction in corneal epithelial cells, suggesting a mechanistic link to spaceflight-induced ocular damage.

### 3.4 | LIUS Attenuates ER Stress and Mitochondrial Dysfunction in SMG-Exposed HCE Cells via the Modulation of MAM Formation

Several ocular drug delivery methods have been developed, including topical eye drops, intravitreal injections, nanoparticle-based systems, and microneedle-mediated administration [51]. However, in spaceflight environments, the altered fluid dynamics caused by microgravity significantly limit the efficacy of conventional topical applications, and invasive approaches such as intravitreal injections may be impractical due to operational constraints [52]. These limitations have created an urgent need for a non-invasive, targeted, and efficient therapeutic strategy for managing ocular damage in space. Recently, LIUS has gained attention as a non-invasive therapeutic modality that can produce beneficial bioeffects through non-thermal mechanisms. To explore its therapeutic potential for spaceflight-relevant ocular injury, we investigated the protective effects and underlying mechanisms of LIUS using an SMG-induced model of corneal epithelial injury.

Cells were cultured in 35 mm dishes and insonated using an ultrasound transducer (Figure S4A). No significant change in temperature was observed after 30 min of LIUS treatment, indicating that LIUS at the applied parameters did not induce detectable thermal effects in the target area (Figure S4B). To assess whether LIUS alone affects HCE cell viability, cells were treated under varying LIUS conditions without the prior application of SMG. A modest reduction in viability was observed at 50 Vpp with 40 kHz stimulation, but it was not statistically significant (Figure S4C). To determine the optimal LIUS parameters for mitigating SMG-induced cell death, HCE cells were exposed to LIUS with varying voltages (5–30 Vpp), frequencies (10–40 kHz), and durations (5–30 min) after 14 days of SMG treatment. Within the 10–20 kHz frequency range, LIUS applied at 10–20 Vpp for 10–30 min significantly attenuated SMG-induced cell death, with the most pronounced protective effect observed under the 20 kHz, 10 Vpp, and 10–30 min conditions. No protective effects were detected at 40 kHz (Figure S4D). Consistent results were obtained from time-course analyses of cell viability under the 30 min LIUS treatment condition, further supporting these findings (Figure S4E). Based on these findings, 10 Vpp and 20 kHz were selected as the optimal LIUS conditions for

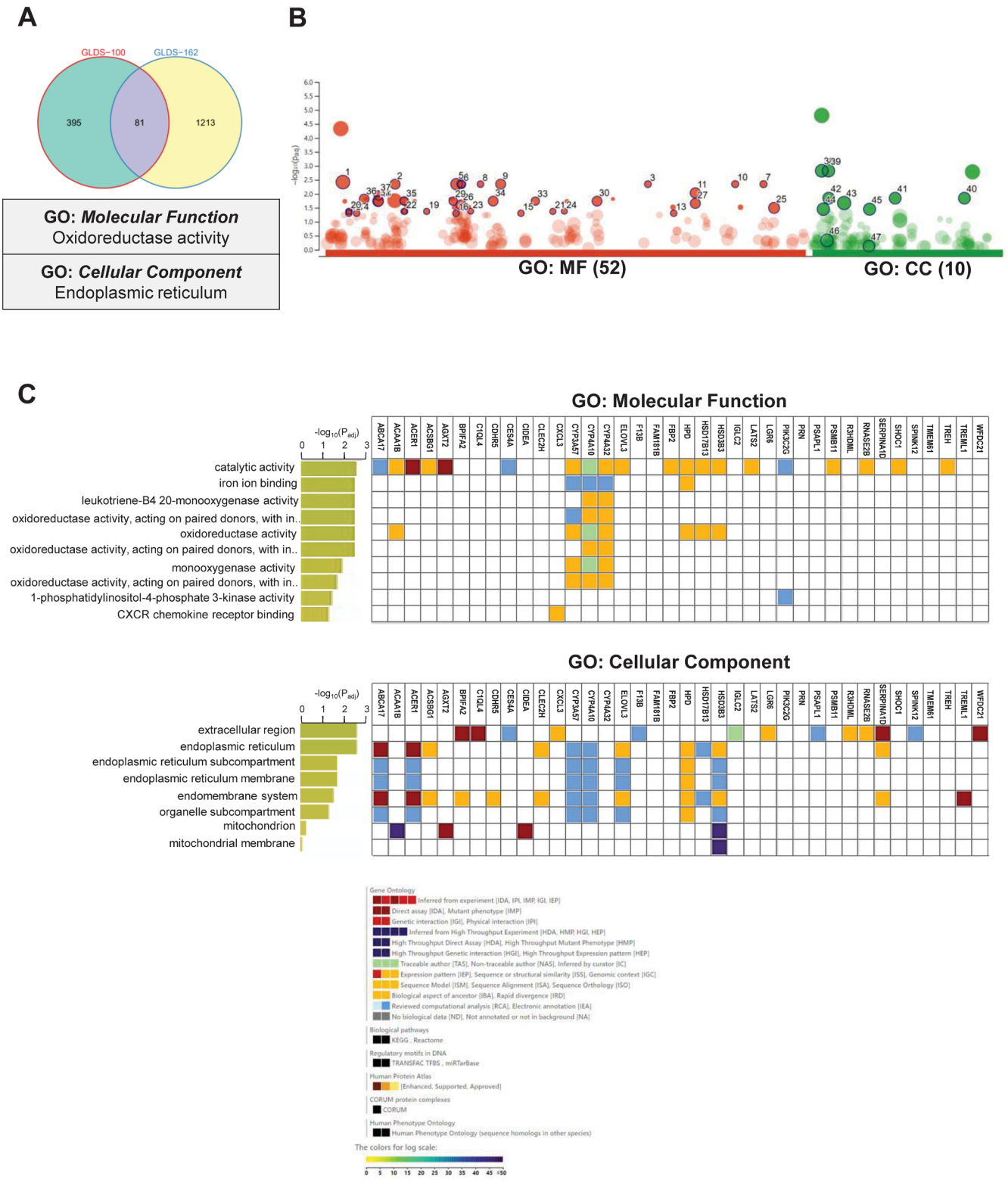


**FIGURE 2** | Transcriptomic profiling of GeneLab datasets reveals microgravity-regulated gene sets. (A) A GSEA was performed on two GeneLab datasets (GLDSs) comparing samples following spaceflight and ground incubation. Venn diagrams display the significantly enriched gene ontology (GO) terms, with overlapping terms summarized in the accompanying table. (B, C) GO enrichment analysis performed using g:Profiler (B). Bubble plot of significantly enriched Molecular Function and Cellular Component categories. Circle size reflects the number of associated genes (C). Summary table of enriched GO terms. Circle size reflects the number of associated genes. Color codes indicate the source of evidence for each annotation.

subsequent experiments. HCE cells were then incubated under 1G or SMG conditions for 7 days and treated daily with LIUS for 30 min (Figure S4F). These LIUS treatments significantly suppressed the SMG-induced upregulation of ER stress–related genes and proteins (Figure 4A,B and Figure S5A). In addition, mitochondrial dysfunction—evidenced by decreased expression

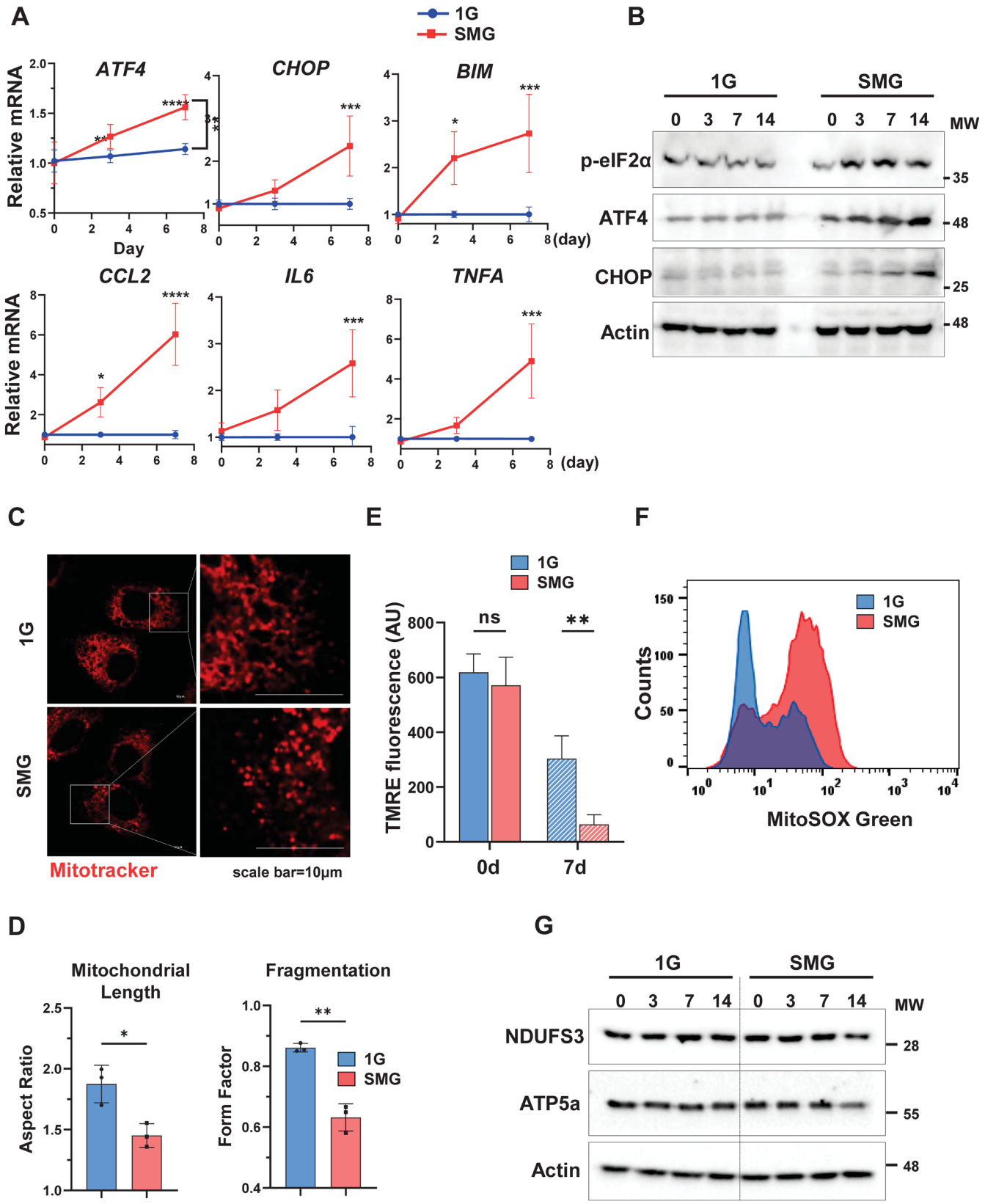


**FIGURE 3** | SMG induces ER stress and mitochondrial dysfunction in HCE cells. (A, B) HCE cells were cultured under 1G or SMG for 7 or 14 days. ER stress-related gene expression was analyzed by RT-qPCR (A) and western blotting (B) analyses. All data are expressed as mean ± SD of three independent experiments. *$p < 0.05$; **$p < 0.01$; ***$p < 0.001$; ****$p < 0.0001$ relative to 1G group (C and D) Mitochondrial morphology visualized by MitoTracker Red CMXRos (250 nM) (C). Measurements of mitochondrial length (aspect ratio) and fragmentation (form factor) are shown in (D). Data are representative of three fields of view per group of three independent experiments. *$p < 0.05$; **$p < 0.01$. (E–G) Mitochondrial membrane potential (TMRE) (E), mitochondrial ROS production (MitoSOX Green) (F), and immunoblot (G) analysis of mitochondrial proteins were measured in 1G- and SMG-treated HCE cells (AU, arbitrary units). Data are presented as mean ± SD of three independent experiments. Ns, not significant; **$p < 0.01$.

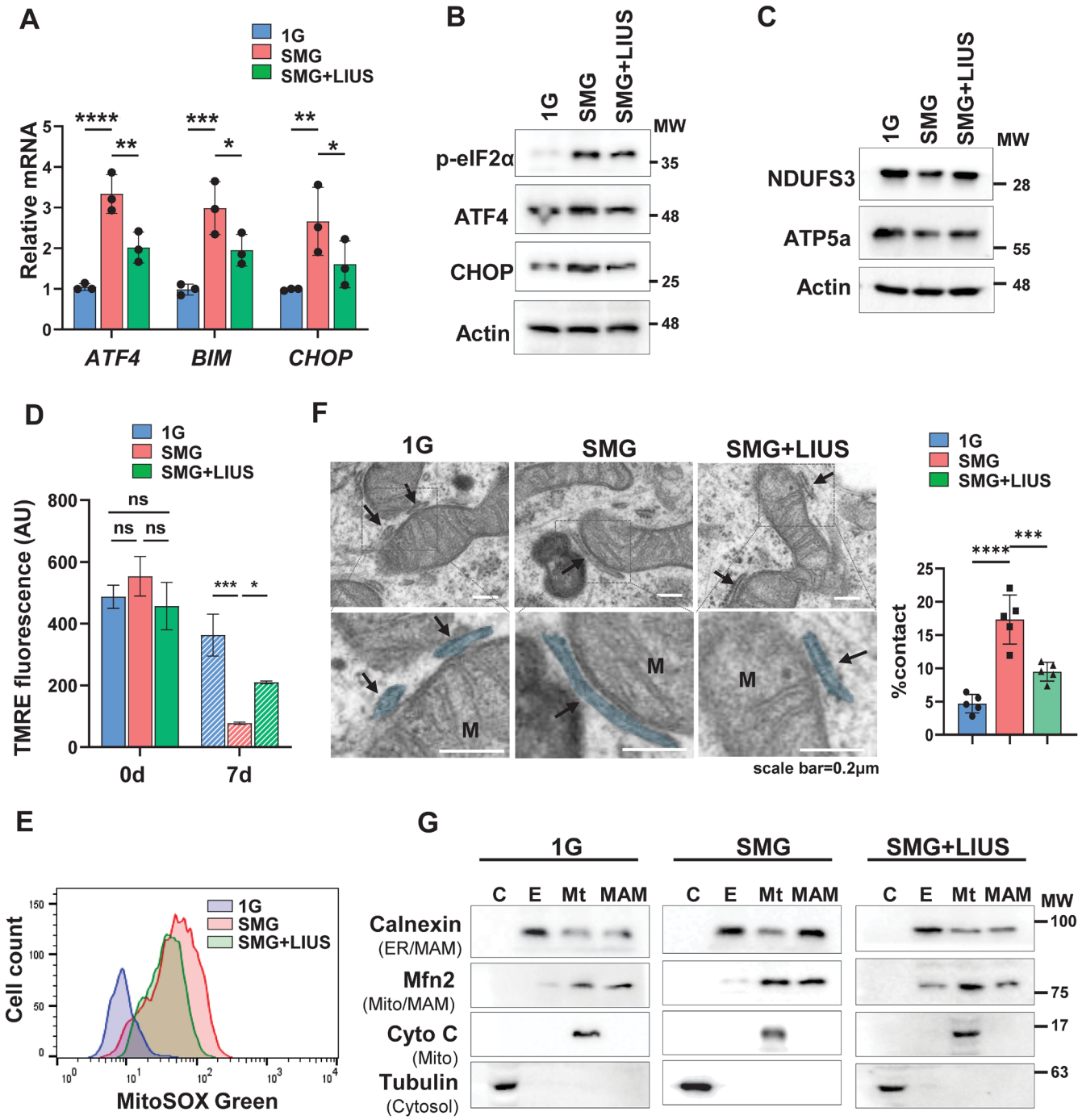


**FIGURE 4** | LIUS attenuates ER stress and mitochondrial dysfunction in SMG-stimulated HCE cells. (A, B) RT-qPCR (A) and immunoblot (B) analyses of ER stress-related genes and proteins, respectively, in 1G- and SMG-treated HCE cells with or without LIUS treatments. Data are expressed as mean ± SD of three independent experiments. *$p < 0.05$; **$p < 0.01$; ***$p < 0.001$; ****$p < 0.0001$. (C–E) Immunoblot (C) analysis of mitochondrial proteins, measurements of mitochondrial membrane potential (TMRE) (D), and ROS production (MitoSOX Green) (E) in 1G- and SMG-treated HCE cells with or without LIUS treatments. Data are expressed as mean ± SD of three independent experiments. *$p < 0.05$; ***$p < 0.001$. (F) Representative electron micrographs showing ER–mitochondria contact points (arrows indicate the ER and "M" denotes mitochondria). The bar graph quantifies the percentage of the mitochondrial surface in close apposition to the ER. Data are expressed as mean ± SD of three independent experiments. ***$p < 0.001$; ****$p < 0.0001$. (G) An immunoblot analysis of selected proteins in four subcellular fractions (C, cytosol; E, ER; Mt., mitochondria; M, MAM) from 1G- and SMG-treated HCE cells with or without LIUS treatments.

of mitochondrial proteins, loss of mitochondrial membrane potential, and increased mitochondrial ROS production—was significantly alleviated by LIUS treatment (Figure 4C–E and Figure S5B), indicating that LIUS effectively mitigates SMG-induced mitochondrial impairment.

To further investigate the mechanism by which LIUS suppresses mitochondrial dysfunction, we focused on its potential effects on membrane microdomains. Previous studies have shown that LIUS can modulate the spatial organization of lipid rafts—cholesterol-rich microdomains that serve as key platforms for

signal transduction—thereby influencing raft-associated signaling pathways [53–55]. Given that MAMs are lipid raft–like domains facilitating inter-organelle communication between the ER and mitochondria [56, 57], we hypothesized that LIUS modulates excessive MAM formation. To test this hypothesis, ER–mitochondria contact points were examined by transmission electron microscopy (TEM). Compared to the 1G group, SMG stimulation significantly increased the length of ER–mitochondrial contact sites, and this increase was markedly reduced by LIUS treatment (Figure 4F). Fluorescence imaging using MitoTracker and ER-Tracker co-staining also revealed a higher degree of colocalization between the ER and mitochondria in SMG-stimulated HCE cells (Figure S5C). To confirm these findings biochemically, we performed Percoll-based subcellular fractionation to isolate mitochondria, ER, and MAM fractions. Consistent with previous findings, calnexin, an ER marker, was enriched in the ER fraction, while cytochrome c and Mfn2 were enriched in the mitochondrial fraction. Notably, when compared to the 1G-group cells, calnexin and Mfn2 levels in the MAM fraction were significantly elevated in SMG-treated HCE cells, suggesting their increased recruitment into MAMs (Figure 4G and Figure S5D). Intriguingly, the LIUS treatments markedly suppressed this effect, indicating an inhibition of the excessive MAM formation process. Collectively, these results suggest that LIUS alleviates SMG-induced mitochondrial dysfunction by attenuating ER–mitochondria coupling through the modulation of MAM organization.

### 3.5 | LIUS Attenuates SMG-Induced Corneal Damage and Promotes Epithelial Repair

Next, we evaluated the efficacy of LIUS in preventing corneal damage under SMG conditions using enucleated mouse eyeballs. Immunofluorescence analysis revealed that the SMG-induced reductions in corneal epithelial nerve fiber density were markedly attenuated by the LIUS treatments (Figure 5A,C). Additionally, LIUS improved epithelial barrier integrity, as evidenced by an increased expression of the tight junction protein ZO-1 and significantly reduced expression levels of MMP9 and VEGF, both of which are associated with barrier disruption and inflammation (Figure 5B–D and Figure S5E). The LIUS treatments also significantly suppressed SMG-induced cell death (Figure 5E). Furthermore, in the scratch wound healing assay, LIUS-treated HCE cells exhibited greater wound closure than the SMG-only group, indicating improved epithelial regeneration (Figure 5F). Taken together, these results demonstrate that LIUS effectively mitigates SMG-induced corneal epithelial damage by preserving epithelial nerve integrity, enhancing barrier function, and promoting wound healing.

## 4 | Discussion

Spaceflight-induced physiological changes pose significant challenges to ocular health, particularly in the maintenance of corneal integrity and function. Despite considerable progress, key knowledge gaps remain—most notably in our understanding of the etiology of corneal damage, the development of effective treatment strategies, and the establishment of reliable ground-based models—as highlighted by the National Aeronautics and Space Administration (NASA) and the European Space Agency (ESA) [58, 59]. In this study, we demonstrated that SMG induces corneal damage through ER stress and mitochondrial dysfunction. Importantly, LIUS effectively reversed this damage by restoring organelle homeostasis and suppressing excessive MAM formation, indicating its potential as a non-invasive therapeutic approach for mitigating spaceflight-induced ocular injury (Figure 6).

One of the most notable findings of our study is that microgravity exacerbates ER stress and mitochondrial dysfunction in HCE cells through the excessive formation of MAMs. Mitochondria-associated membranes function as key platforms for inter-organelle communication, facilitating calcium transfer and lipid exchange and regulating mitochondrial dynamics. While MAMs support cellular homeostasis, pathological expansion of these structures has been implicated in oxidative stress and apoptotic signaling due to calcium overload and sustained mitochondrial dysfunction. Transmission electron microscopy and biochemical fractionation revealed increased ER–mitochondrial contact and the upregulation of MAM-localized proteins, such as calnexin and Mfn2, under SMG, supporting the notion that dysregulated MAM formation contributes to organelle stress and cell death in this context. These results are in line with recent studies reporting MAM dysregulation in ocular diseases, including glaucoma, corneal dystrophy, and retinal degeneration [60, 61]. Our results thus provide novel mechanistic insights into the mitochondrial vulnerability observed during spaceflight and underscore the previously underappreciated role of MAMs as a therapeutic target in mitigating spaceflight-induced cellular stress.

Although mitochondrial dysfunction appears to play a central role in SMG-induced corneal epithelial injury and neuronal cell death, these phenomena may represent an integrated outcome of multiple signaling pathway alterations and microenvironmental changes. Transcriptomic analyses of mouse eye samples obtained from spaceflight missions [9, 10, 62] and from ground-based microgravity models such as hindlimb unloading mice [63] have demonstrated significant enrichment not only in mitochondrial processes but also in pathways related to innate immunity and chronic inflammation. Inflammatory responses, ER stress, and mitochondrial function are closely interrelated. Previous studies have shown that NALP3 inflammasome activation and microglial reactivity are linked to mitochondrial dysfunction [64, 65], while mitochondrial damage can, in turn, trigger mtDNA release and activate the cGAS–STING pathway and NALP3 inflammasome [66, 67]. Notably, NALP3 has been reported to redistribute to MAMs for inflammasome assembly [68], supporting the notion that ER stress–induced MAM expansion, as observed in this study, may play a critical role in mediating inflammation and mitochondrial injury. Future studies should therefore further elucidate these signaling interactions and investigate how macrophage- and myeloid cell–driven inflammatory microenvironmental changes contribute to ocular pathology under SMG conditions [69]. Single-cell profiling using SMG-induced animal models such as hindlimb unloading mice will be valuable for defining temporal dynamics of ocular cell subsets, dissecting inter-pathway relationships, and determining how LIUS modulates these processes.

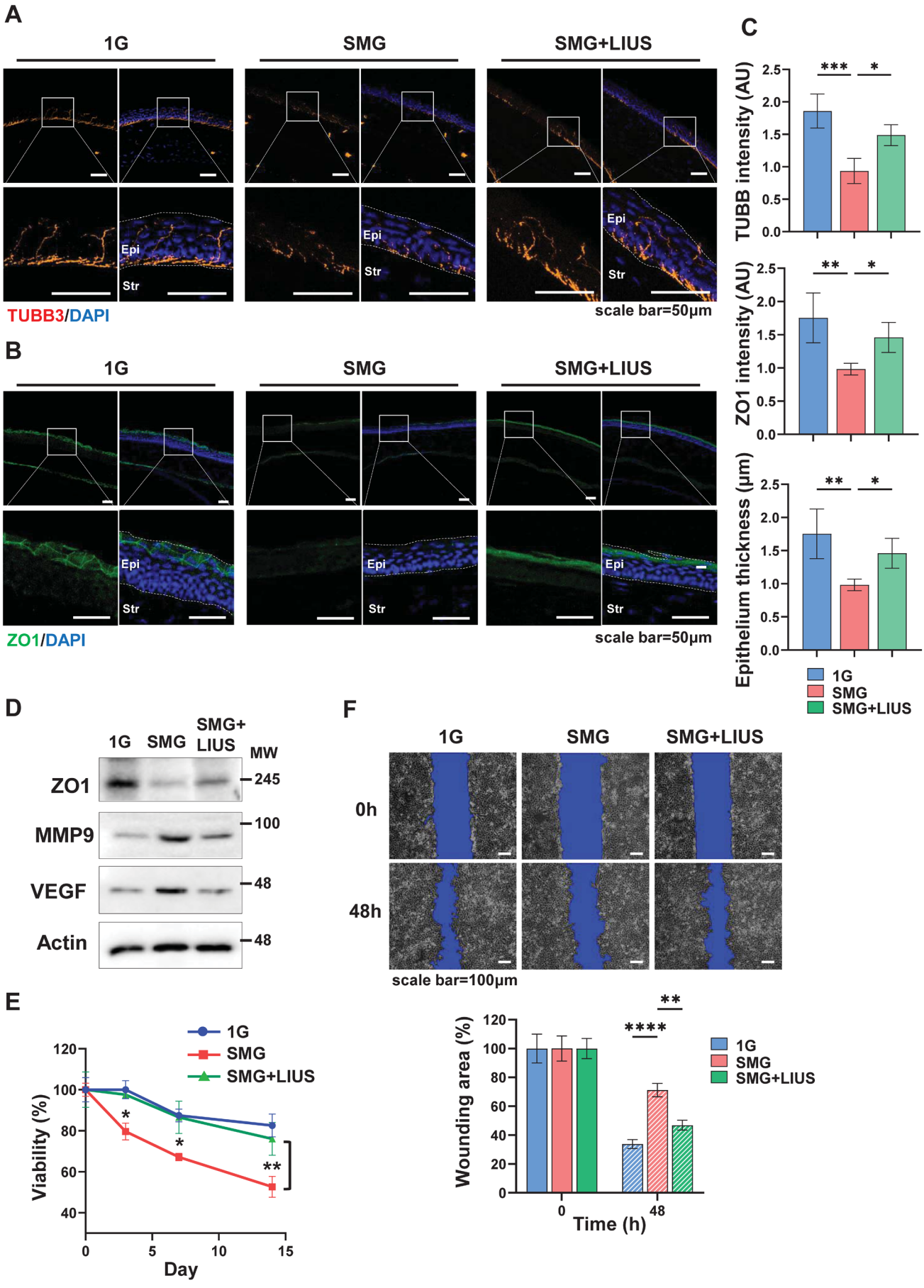


**FIGURE 5** | Legend on next page.

**FIGURE 5** | LIUS mitigates SMG-induced corneal damage. (A–C) The confocal immunohistochemistry of corneal sections from SMG- and 1G-exposed eyeballs treated with or without LIUS, including representative images of TUBB3 (A) and ZO-1 (B) staining. Measurements of fluorescence intensity are shown in (C). Eyes from three mice per group were examined, and data are representative of three fields of view per group of three independent experiments. *$p < 0.05$; **$p < 0.01$; ***$p < 0.001$. (D) A western blot analysis of selected proteins extracted from HCE cells cultured under 1G or SMG conditions with or without LIUS treatment. (E) The cell viability of HCE cells after LIUS treatment under 1G or SMG conditions, assessed via WST-8 assays. Data are expressed as mean ± SD of three independent experiments. *$p < 0.05$; **$p < 0.01$. (F) Scratch assays were performed on confluent HCE monolayers followed by a 48-h incubation. Representative images (top) and measurements of wound area (bottom) are shown. Data are expressed as mean ± SD of three independent experiments. **$p < 0.01$; ****$p < 0.0001$.

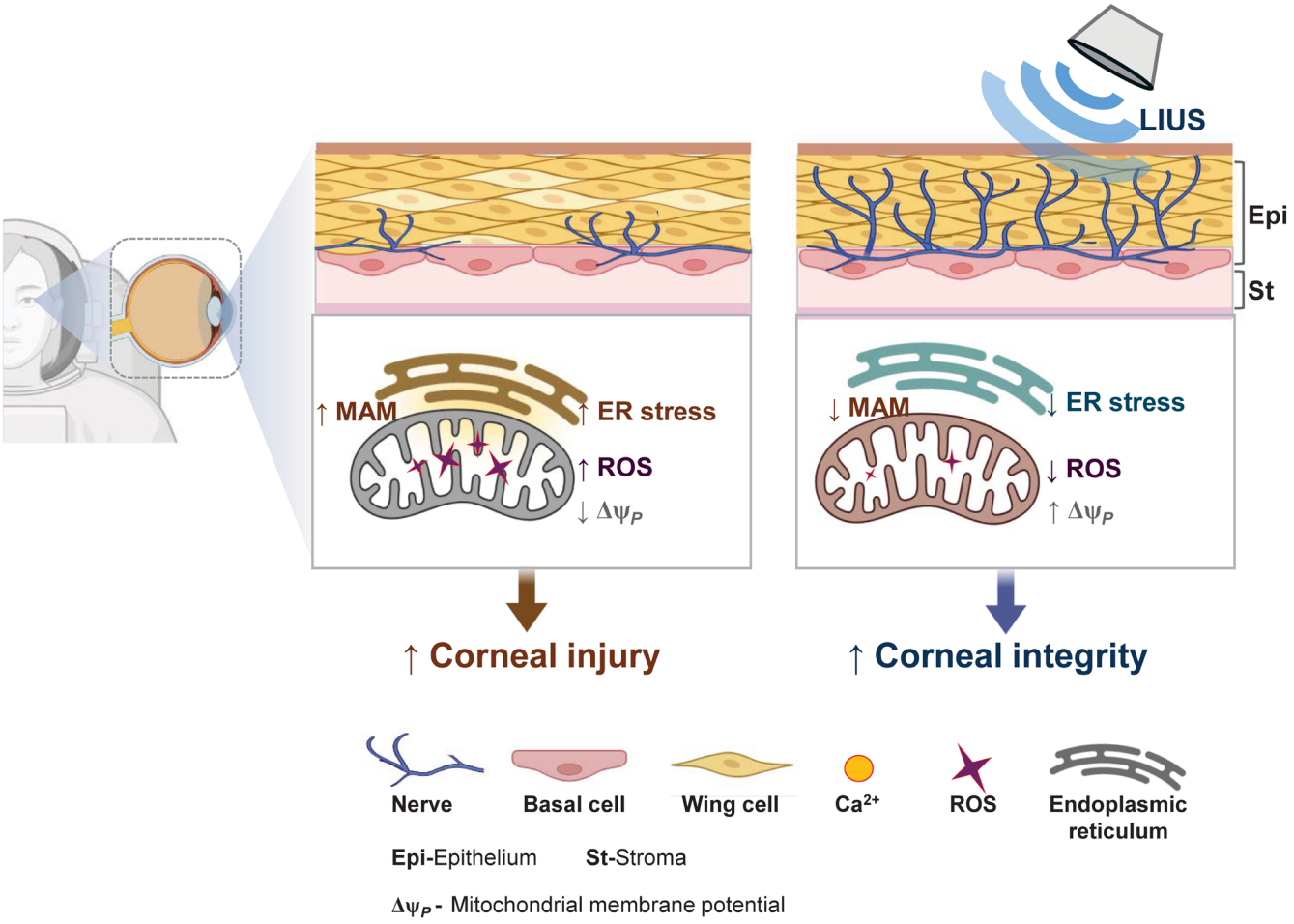


**FIGURE 6** | Schematic representation of LIUS-mediated protection against SMG-induced corneal injury. Simulated microgravity provokes corneal epithelial and neural cell injury by heightened ER stress, mitochondrial dysfunction, and aberrant formation of MAMs. Low-intensity ultrasound treatment counteracts this pathological cascade by normalizing MAM dynamics, thereby relieving organelle stress and promoting cellular survival.

Low-intensity ultrasound has shown therapeutic potential across a range of medical applications due to its ability to modulate biological responses through non-thermal mechanical stimulation. In this study, we show that LIUS treatments, when applied using optimized parameters (10 Vpp and 20 kHz), significantly attenuate SMG-induced ER stress and mitochondrial dysfunction in HCE cells. Notably, LIUS also suppressed excessive MAM formation and reduced ER–mitochondria coupling, suggesting that its cytoprotective effects involve the remodeling of subcellular membrane microdomains. This is supported by previous studies reporting that LIUS can modulate lipid raft organization and raft-associated signaling pathways [53–55]. Beyond molecular effects, LIUS exerted significant protective effects at the tissue level. The LIUS treatments restored epithelial nerve fiber density, upregulated tight junction protein ZO-1, a protein critical for epithelial structural integrity, and reduced the expression of MMP9 and VEGF, markers linked to epithelial barrier breakdown and inflammation. Moreover, LIUS improved cell viability and accelerated wound closure in scratch assays under SMG conditions.

In this study, our results collectively demonstrate that LIUS not only mitigates stress responses but also promotes functional epithelial regeneration. This multi-level protection underscores its potential as a non-invasive, adaptable, and clinically relevant countermeasure for spaceflight-induced ocular pathology. Considering the limitations of topical drug delivery under microgravity and the impracticality of invasive ocular interventions in space, LIUS represents a compelling alternative for

maintaining astronauts' ocular health. Future studies should evaluate the long-term safety and efficacy of LIUS in vivo and explore its application for other spaceflight-related disorders. Additionally, mechanistic studies on lipid raft modulation and MAM-associated signaling pathways will be critical to further elucidating the molecular basis of LIUS-mediated protection.

## 5 | Conclusion

This study identifies a previously uncharacterized mechanism by which simulated microgravity induces corneal injury, highlighting the pathological role of excessive MAM formation in driving ER stress and mitochondrial dysfunction. Notably, LIUS attenuated these stress responses by modulating MAM dynamics, thereby preserving cellular viability. These findings support LIUS as a promising non-invasive intervention to mitigate microgravity-induced ocular damage and underscore the importance of targeting inter-organelle communication pathways to maintain visual health during long-duration spaceflight.

### Author Contributions

J.H.L. and D.Y.K. conceptualized and designed the study. J.H.L. performed the biological experiments, analyzed the data, and prepared the figures and tables. H.K. established the low-intensity ultrasound system and conducted preliminary experiments. J.H.L. and D.Y.K. wrote and revised the manuscript. D.Y.K. supervised the overall project. All authors reviewed and approved the final version of the manuscript.


### Acknowledgments

This research was supported by the National Research Foundation of Korea (RS-2025-16071542, RS-2018-NR031065 and RS-2023-NR076534), by the Korea Medical Device Development Fund grant funded by the Korea government (the Ministry of Science and ICT, the Ministry of Trade, Industry and Energy, the Ministry of Health & Welfare, the Ministry of Food and Drug Safety) (Project Number: RS-2023-00242778).

### Funding

This work was supported by National Research Foundation of Korea (NRF), RS-2018-NR031065, RS-2023-NR076534; Korea Medical Device Development Fund (KMDF), RS-2023-00242778; National Research Foundation of Korea (NRF), RS-2025-16071542.


### Conflicts of Interest

The authors declare no conflicts of interest.

### Data Availability Statement

All data relevant to the study are included in the article or as Appendix S1. Upon reasonable request, additional information (e.g., protocols) will be shared by the corresponding authors.

### References


1. K. G. Sreejalekshmi, "Space Biosciences: Translational Research for Space, Benefitting Life on Earth," in *Translational Research in Biomedical Sciences: Recent Progress and Future Prospects*, ed. K. Parthasarathy and R. Manikkam (Springer Nature Singapore, 2024), 31–43.

2. X. Zhang, G. Wang, S. Zhang, et al., "Genomes of the Banyan Tree and Pollinator Wasp Provide Insights Into Fig-Wasp Coevolution," *Cell* 183 (2020): 875–889.

3. G. C. Demontis, M. M. Germani, E. G. Caiani, I. Barravecchia, C. Passino, and D. Angeloni, "Human Pathophysiological Adaptations to the Space Environment," *Frontiers in Physiology* 8 (2017): 547.

4. A. G. Lee, T. H. Mader, C. R. Gibson, et al., "Spaceflight Associated Neuro-Ocular Syndrome (SANS) and the Neuro-Ophthalmologic Effects of Microgravity: A Review and an Update," *Npj Microgravity* 6 (2020): 7.

5. J. Ong, B. Soares, D. Osteicoechea, et al., "The Cornea During Spaceflight: A Frontier in Space Medicine Ophthalmology," *Eye (London, England)* 38 (2024): 3207–3209.

6. N. Panzo, H. Memon, J. Ong, et al., "Molecular and Biomechanical Changes of the Cornea and Lens in Spaceflight," *Life Sciences in Space Research* 45 (2025): 151–157.

7. H. P. Nguyen, P. H. Tran, K.-S. Kim, and S.-G. Yang, "The Effects of Real and Simulated Microgravity on Cellular Mitochondrial Function," *Npj Microgravity* 7 (2021): 44.

8. B. J. Feger, J. W. Thompson, L. G. Dubois, et al., "Microgravity Induces Proteomics Changes Involved in Endoplasmic Reticulum Stress and Mitochondrial Protection," *Scientific Reports* 6 (2016): 34091.

9. W. A. da Silveira, H. Fazelinia, S. B. Rosenthal, et al., "Comprehensive Multi-Omics Analysis Reveals Mitochondrial Stress as a Central Biological Hub for Spaceflight Impact," *Cell* 183 (2020): 1185–1201.

10. C. A. Theriot and S. B. Zanello, "Molecular Effects of Spaceflight in the Mouse Eye After Space Shuttle Mission STS-135," *Gravitational and Space Research* 2 (2014): 3–24.

11. W. Ouyang, D. Yan, J. Hu, and Z. Liu, "Multifaceted Mitochondrial as a Novel Therapeutic Target in Dry Eye: Insights and Interventions," *Cell Death Discovery* 10 (2024): 398.

12. B. S. Chen, J. P. Harvey, M. J. Gilhooley, N. Jurkute, and P. Yu-Wai-Man, "Mitochondria and the Eye—Manifestations of Mitochondrial Diseases and Their Management," *Eye* 37 (2023): 2416–2425.

13. J. H. Pham and D. L. Stankowska, "Mitochondria-Associated Endoplasmic Reticulum Membranes (MAMs) and Their Role in Glaucomatous Retinal Ganglion Cell Degeneration—A Mini Review," *Frontiers in Neuroscience* 17 (2023): 1198343.

14. M. Giacomello and L. Pellegrini, "The Coming of Age of the Mitochondria–ER Contact: A Matter of Thickness," *Cell Death and Differentiation* 23 (2016): 1417–1427.

15. S. Missiroli, S. Patergnani, N. Caroccia, et al., "Mitochondria-Associated Membranes (MAMs) and Inflammation," *Cell Death & Disease* 9 (2018): 329.

16. A. R. van Vliet and P. Agostinis, "Mitochondria-Associated Membranes and ER Stress," *Current Topics in Microbiology and Immunology* 414 (2018): 73–102.

17. J. D. Malhotra and R. J. Kaufman, "ER Stress and Its Functional Link to Mitochondria: Role in Cell Survival and Death," *Cold Spring Harbor Perspectives in Biology* 3 (2011): a004424.

18. S. Patergnani, J. M. Suski, C. Agnoletto, et al., "Calcium Signaling Around Mitochondria Associated Membranes (MAMs)," *Cell Communication and Signaling* 9 (2011): 19.

19. B. Kaur, B. Miglioranza Scavuzzi, M. Yang, et al., "ER Stress and Mitochondrial Perturbations Regulate Cell Death in Retinal Detachment: Exploring the Role of HIF1α," *Investigative Ophthalmology & Visual Science* 65 (2024): 39.

20. S. Qureshi, S. Lee, W. Steidl, et al., "Endoplasmic Reticulum Stress Disrupts Mitochondrial Bioenergetics, Dynamics and Causes Corneal

Endothelial Cell Apoptosis," *Investigative Ophthalmology & Visual Science* 64 (2023): 18.

21. D. L. Miller, N. B. Smith, M. R. Bailey, G. J. Czarnota, K. Hynynen, and I. R. Makin, "Overview of Therapeutic Ultrasound Applications and Safety Considerations," *Journal of Ultrasound in Medicine* 31 (2012): 623–634.

22. J. Sapoval, V. Singh, and R. E. Carter, "Ultrasound Biophysical Profile(Archived)," in *StatPearls* (StatPearls Publishing, 2025).

23. M. Daffertshofer and M. Fatar, "Therapeutic Ultrasound in Ischemic Stroke Treatment: Experimental Evidence," *European Journal of Ultrasound* 16 (2002): 121–130.

24. S. Takikawa, N. Matsui, T. Kokubu, et al., "Low-Intensity Pulsed Ultrasound Initiates Bone Healing in Rat Nonunion Fracture Model," *Journal of Ultrasound in Medicine* 20 (2001): 197–205.

25. P. Bowary and B. D. Greenberg, "Noninvasive Focused Ultrasound for Neuromodulation: A Review," *Psychiatric Clinics of North America* 41 (2018): 505–514.

26. A. K. Wood and C. M. Sehgal, "A Review of Low-Intensity Ultrasound for Cancer Therapy," *Ultrasound in Medicine & Biology* 41 (2015): 905–928.

27. X. Jiang, O. Savchenko, Y. Li, et al., "A Review of Low-Intensity Pulsed Ultrasound for Therapeutic Applications," *IEEE Transactions on Biomedical Engineering* 66 (2019): 2704–2718.

28. Z. Sun, Z. Li, J. T. Chung, L. C. M. Lau, V. Jhanji, and Y. Chau, "Low-Intensity Low-Frequency Ultrasound Mediates Riboflavin Delivery During Corneal Crosslinking," *Bioengineering & Translational Medicine* 8 (2023): e10442.

29. J.-X. Zhou, Y.-J. Liu, X. Chen, et al., "Low-Intensity Pulsed Ultrasound Protects Retinal Ganglion Cell From Optic Nerve Injury Induced Apoptosis via Yes Associated Protein," *Frontiers in Cellular Neuroscience* 12 (2018): 160.

30. T. Wang, M. Wang, J. Wang, Z. Li, and Y. Yuan, "Modulatory Effects of Low-Intensity Retinal Ultrasound Stimulation on Rapid and Non-Rapid Eye Movement Sleep," *Cerebral Cortex* 34 (2024): bhae143.

31. M. Du, Y. Li, Q. Zhang, J. Zhang, S. Ouyang, and Z. Chen, "The Impact of Low Intensity Ultrasound on Cells: Underlying Mechanisms and Current Status," *Progress in Biophysics and Molecular Biology* 174 (2022): 41–49.

32. T.-T. Truong, C.-C. Huang, and W.-T. Chiu, "Low-Intensity Pulsed Ultrasound Reduces Oxidative and Endoplasmic Reticulum Stress in Motor Neuron Cells," *Ultrasonics* 146 (2025): 107499.

33. J. Li, Q. Zhang, C. Ren, et al., "Low-Intensity Pulsed Ultrasound Prevents the Oxidative Stress Induced Endothelial-Mesenchymal Transition in Human Aortic Endothelial Cells," *Cellular Physiology and Biochemistry* 45 (2018): 1350–1365.

34. Q. Cao, L. Liu, Y. Hu, et al., "Low-Intensity Pulsed Ultrasound of Different Intensities Differently Affects Myocardial Ischemia/Reperfusion Injury by Modulating Cardiac Oxidative Stress and Inflammatory Reaction," *Frontiers in Immunology* 14 (2023): 1248056.

35. M. Chang, L. Zhang, T. Zhang, et al., "Ultrasound-Augmented Enzyodynamic-Ca2+ Overload Synergetic Tumor Nanotherapy," *Biomaterials* 307 (2024): 122513.

36. W. Zhong, X. Chen, P. Jiang, J. M. Wan, P. Qin, and A. C. Yu, "Induction of Endoplasmic Reticulum Stress by Sonoporation: Linkage to Mitochondria-Mediated Apoptosis Initiation," *Ultrasound in Medicine & Biology* 39 (2013): 2382–2392.

37. S. Gustmann and N. Dünker, "In Vivo-Like Organotypic Murine Retinal Wholemount Culture," *Journal of Visualized Experiments* 35 (2010): e1634.

38. A. Fernandes, N. D. Mendes, G. M. Almeida, et al., "Short-Term Free-Floating Slice Cultures From the Adult Human Brain," *Journal of Visualized Experiments* 153 (2019): e59845.

39. T. Otsuka, T. Imura, K. Nakagawa, et al., "Simulated Microgravity Culture Enhances the Neuroprotective Effects of Human Cranial Bone-Derived Mesenchymal Stem Cells in Traumatic Brain Injury," *Stem Cells and Development* 27 (2018): 1287–1297.

40. T. Furukawa, K. Tanimoto, T. Fukazawa, T. Imura, Y. Kawahara, and L. Yuge, "Simulated Microgravity Attenuates Myogenic Differentiation via Epigenetic Regulations," *Npj Microgravity* 4 (2018): 11.

41. J. H. Lee and D. Y. Kim, "25-Hydroxysterol Mitigates Microgravity-Induced Retinal Damage by Suppressing Microglial Inflammation Through Disrupting Lipid Raft Formation," *Npj Microgravity* 11 (2025): 49.

42. M. T. Tran, C. N. Q. Ho, S. N. Hoang, et al., "Morphological Changes of 3T3 Cells Under Simulated Microgravity," *Cells* 13 (2024): 123.

43. T. X. Dai, H. N. Son, H. N. Q. Chi, et al., "Simulated Microgravity Induces the Proliferative Inhibition and Morphological Changes in Porcine Granulosa Cells," *Current Issues in Molecular Biology* 43 (2021): 2210–2219.

44. M. R. Wieckowski, C. Giorgi, M. Lebiedzinska, J. Duszynski, and P. Pinton, "Isolation of Mitochondria-Associated Membranes and Mitochondria From Animal Tissues and Cells," *Nature Protocols* 4 (2009): 1582–1590.

45. G. Di, X. Qi, X. Zhao, S. Zhang, P. Danielson, and Q. Zhou, "Corneal Epithelium-Derived Neurotrophic Factors Promote Nerve Regeneration," *Investigative Ophthalmology & Visual Science* 58 (2017): 4695–4702.

46. L. J. Müller, C. F. Marfurt, F. Kruse, and T. M. T. Tervo, "Corneal Nerves: Structure, Contents and Function," *Experimental Eye Research* 76 (2003): 521–542.

47. W. Philipp, L. Speicher, and C. Humpel, "Expression of Vascular Endothelial Growth Factor and Its Receptors in Inflamed and Vascularized Human Corneas," *Investigative Ophthalmology & Visual Science* 41 (2000): 2514–2522.

48. D. Q. Li, B. L. Lokeshwar, A. Solomon, D. Monroy, Z. Ji, and S. C. Pflugfelder, "Regulation of MMP-9 Production by Human Corneal Epithelial Cells," *Experimental Eye Research* 73 (2001): 449–459.

49. B. S. Kowtharapu, T. Stahnke, A. Wree, R. F. Guthoff, and O. Stachs, "Corneal Epithelial and Neuronal Interactions: Role in Wound Healing," *Experimental Eye Research* 125 (2014): 53–61.

50. V. Kumar, "Endoplasmic Reticulum-Mitochondrial Cross-Talk in Neurodegenerative and Eye Diseases," *Neurology (ECronicon)* 11 (2019): 864–873.

51. V. Gote, S. Sikder, J. Sicotte, and D. Pal, "Ocular Drug Delivery: Present Innovations and Future Challenges," *Journal of Pharmacology and Experimental Therapeutics* 370 (2019): 602–624.

52. H. Memon, J. Ong, E. Waisberg, et al., "Biophysics of Ophthalmic Medications During Spaceflight: Principles of Ocular Fluid Dynamics and Pharmacokinetics in Microgravity," *Life Sciences in Space Research* 42 (2024): 53–61.

53. E. F. Small, N. R. Dan, and S. P. Wrenn, "Low-Frequency Ultrasound-Induced Transport Across Non-Raft-Forming Ternary Lipid Bilayers," *Langmuir* 28 (2012): 14364–14372.

54. E. F. Small, M. C. Willy, P. A. Lewin, and S. P. Wrenn, "Ultrasound-Induced Transport Across Lipid Bilayers: Influence of Phase Behavior," *Colloids and Surfaces A: Physicochemical and Engineering Aspects* 390 (2011): 40–47.

55. M. L. Prieto, O. Ömer, B. T. Khuri-Yakub, and M. C. Maduke, "Dynamic Response of Model Lipid Membranes to Ultrasonic Radiation Force," *PLoS One* 8 (2013): e77115.

56. T. Garofalo, P. Matarrese, V. Manganelli, et al., "Evidence for the Involvement of Lipid Rafts Localized at the ER-Mitochondria Associated

Membranes in Autophagosome Formation," *Autophagy* 12 (2016): 917–935.

57. E. Area-Gomez, M. Del Carmen Lara Castillo, M. D. Tambini, et al., "Upregulated Function of Mitochondria-Associated ER Membranes in Alzheimer Disease," *EMBO Journal* 31 (2012): 4106–4123.

58. A. P.-L. Traon, L. Petersen, Y. Y. Stern, and P. z. Eulenburg, "ESA SciSpacE White Papers, #12," Human Physiology, (2021).

59. S. S. Laurie, B. R. Macias, L. P. Pardon, et al., "Risk of Spaceflight Associated Neuro-Ocular Syndrome (SANS)," (2022).

60. X.-Y. Zhang, C. Han, Y. Yao, and T.-T. Wei, "Current Insights on Mitochondria-Associated Endoplasmic Reticulum Membranes (MAMs) and Their Significance in the Pathophysiology of Ocular Disorders," *Experimental Eye Research* 248 (2024): 110110.

61. J. J. Wang, K. S. Park, N. Dhimal, et al., "Proteomic Analysis of Retinal Mitochondria-Associated ER Membranes Identified Novel Proteins of Retinal Degeneration in Long-Term Diabetes," *Cells* 11 (2022): 459.

62. S. B. Zanello, C. A. Theriot, C. M. P. Ponce, and P. Chevez-Barrios, "Spaceflight Effects and Molecular Responses in the Mouse Eye: Preliminary Observations After Shuttle Mission STS-133," *Gravitational and Space Research* 1 (2013): 29–46.

63. P. Kothiyal, G. Eley, H. Ilangovan, et al., "A Multi-Omics Longitudinal Study of the Murine Retinal Response to Chronic Low-Dose Irradiation and Simulated Microgravity," *Scientific Reports* 12 (2022): 16825.

64. M. E. Heid, P. A. Keyel, C. Kamga, S. Shiva, S. C. Watkins, and R. D. Salter, "Mitochondrial Reactive Oxygen Species Induces NLRP3-Dependent Lysosomal Damage and Inflammasome Activation," *Journal of Immunology* 191 (2013): 5230–5238.

65. M. J. Lopez-Armada, R. R. Riveiro-Naveira, C. Vaamonde-Garcia, and M. N. Valcarcel-Ares, "Mitochondrial Dysfunction and the Inflammatory Response," *Mitochondrion* 13 (2013): 106–118.

66. E. Latz, T. S. Xiao, and A. Stutz, "Activation and Regulation of the Inflammasomes," *Nature Reviews. Immunology* 13 (2013): 397–411.

67. A. P. West and G. S. Shadel, "Mitochondrial DNA in Innate Immune Responses and Inflammatory Pathology," *Nature Reviews. Immunology* 17 (2017): 363–375.

68. R. Zhou, A. S. Yazdi, P. Menu, and J. Tschopp, "A Role for Mitochondria in NLRP3 Inflammasome Activation," *Nature* 469 (2011): 221–225.

69. P. Wieghofer, N. Hagemeyer, R. Sankowski, et al., "Mapping the Origin and Fate of Myeloid Cells in Distinct Compartments of the Eye by Single-Cell Profiling," *EMBO Journal* 40 (2021): e105123.

**Supporting Information**

Additional supporting information can be found online in the Supporting Information section. **Appendix S1:** fsb271462-sup-0001-Supinfo.pdf.